JOURNAL OF OPTOELECTRONICS AND ADVANCED MATERIALS Vol. 10, No. 6, June 2008, p. 1442 - 1447

Three-dimensional analysis of electric current distribution in a small-scale scramjet driven DCW MHD generator

MOTOO ISHIKAWA*, DAIKI GOTOH, TORU TAKAHASHI, TAKAYASU FUJINO♣
Graduate School of Systems and Information Engineering, University of Tsukuba
Tsukuba, 305-8573, Japan

An experimental scramjet driven MHD generator developed under the Hypersonic Vehicle Electric Power System (HVEPS) program has been numerically simulated and analyzed using a fully coupled three dimensional MHD generator computer code. The three dimensional simulations have shown very good agreement between the experimental and numerical results in the active MHD region when a scalar electrical conductivity deficit of 81.3% of ideal is imposed. The major power performance loss mechanism identified in the three dimensional simulation is relatively large near electrode voltage drops on the order of 100 Volts with a ratio to the induced MHD voltage of about 0.3. The analysis shows detail of rather strong eddy-like current that is induced in PTO regions. This eddy-like current may interact with the load current running in and out of the PTO frames, resulting in the power degradation.

(Received March 13, 2008; accepted after revision June 4, 2008)

Keywords: Scramjet driven DCW MHD generator, Three-dimensional analysis, Power take-off region, Electrode voltage drop, Eddy current

1. Introduction

The scramjet driven magnetohydrodynamics (MHD) generation has been proposed as a high electric power source on an advanced hypersonic aircraft. A full-scale hypersonic vehicle requires an on-board high electric power source. In general, 1's to 10's of megawatts of electric power are thought as being necessary to excite the EM/MHD interactions levels necessary to allow significant aero improvements[1), 2)]. Then, the Hypersonic Vehicle Electric Power System (HVEPS) program was started as a five-year research and development plan that was lead by General Atomics Corporation with consignments to Ly-Tec, The University of Tennessee Space Institute, and Pratt Whitney Rocketdyne (PWR) for the MHD power system development. Descriptions of the HVEPS program and summaries of the work concluded under that program are detailed in References 1, 2 and 3.

The scramjet-driven MHD power concept is based on the cycle which utilizes the high temperature hypersonic inlet flow air stream as oxidizer with near stoichiometric scramjet combustion to produce the temperatures required to promote the MHD power process. The addition of ionization seeding material (alkali metal) to the stream produces an electrically conducting plasma exhaust that passes to the MHD generator which produces useful external electric power by MHD interaction.

In December of 2006, the HVEPS scramjet MHD power demonstration test was successfully concluded. Two series of test were conducted and significant MHD power production was achieved in all individual tests of these series. Reference 3 is the most recent publication on this subject as was produced by the HVEPS research team and provides fundamental characterization of the demonstrated MHD electrical performance based on classical MHD theory. Preliminary three-dimensional analysis with very interesting results is reported in Ref. (4).

Fig. 1 provides a schematic of the MHD generator, which was located centrally inside the bore of the circular superconducting magnet coils. The scramjet engine was supplied with simulated Mach 8 air stream using a high pressure H2-O2 preheater. Ionization seed was injected into the hot air stream in the upstream pre-heater using liquid NaK to allow for its dissociation, vaporization and thorough mixing prior to the scramjet combustion.

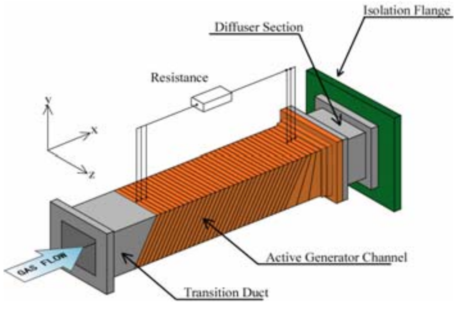

Fig. 1 MHD generator channel loading schematic.

The present paper intends to show current distributions in the MHD channel and to reveal the reason of performance degradation near inlet and outlet power take-off

---

♣Paper communicated to the 5th Japonese-Mediterranean workshop on Applied Engineering for Magnetic Superconducting and Nanomaterials, September 16-19, 2007, Larnaca, Cyprus, Greece

(PTO) regions found by the recent experiments with fully coupled three-dimensional analysis of fluid dynamics and electrodynamics.

2. Mathematical models

2.1 Basic equations

Gasdynamics

The conservation forms of time-dependent three-dimensional compressible equations are used for gasdynamics. The algebraic model proposed by Stock and Haase[5)] is used as a turbulence model.

$$\frac{\partial \mathbf{Q}}{\partial \mathrm{t}}+\frac{\partial \mathbf{F}}{\partial \mathrm{x}}+\frac{\partial \mathbf{G}}{\partial \mathrm{y}}+\frac{\partial \mathbf{H}}{\partial \mathrm{z}} +\frac{\partial \mathbf{F}_{\mathrm{v}}}{\partial \mathrm{x}}+\frac{\partial \mathbf{G}_{\mathrm{v}}}{\partial \mathrm{y}}+\frac{\partial \mathbf{H}_{\mathrm{v}}}{\partial \mathrm{z}}+\mathbf{S}=\mathbf{0} \tag{1}$$

$$\mathbf{Q}=\begin{pmatrix}\rho\\ \rho u\\ \rho v\\ \rho w\\ e\end{pmatrix} \quad \mathbf{F}=\begin{pmatrix}\rho u\\ \rho u^2+p\\ \rho uv\\ \rho uw\\ (e+p)u\end{pmatrix} \quad \mathbf{G}=\begin{pmatrix}\rho v\\ \rho vu\\ \rho v^2+p\\ \rho vw\\ (e+p)v\end{pmatrix}$$

$$\mathbf{H}=\begin{pmatrix}\rho w\\ \rho wu\\ \rho wv\\ \rho w^2+p\\ (e+p)w\end{pmatrix} \quad \mathbf{S}=\begin{pmatrix}0\\ -J_yB\\ J_xB\\ 0\\ -\mathbf{J}\cdot\mathbf{E}\end{pmatrix}$$

$$\mathbf{F}_v=-\begin{pmatrix}0\\ \tau_{xx}\\ \tau_{yx}\\ \tau_{zx}\\ u\tau_{xx}+v\tau_{xy}+w\tau_{xz}+k_e\frac{\partial T}{\partial x}\end{pmatrix}$$

$$\mathbf{G}_v=-\begin{pmatrix}0\\ \tau_{xy}\\ \tau_{yy}\\ \tau_{zy}\\ u\tau_{yx}+v\tau_{yy}+w\tau_{yz}+k_e\frac{\partial T}{\partial y}\end{pmatrix}$$

$$\mathbf{H}_v=-\begin{pmatrix}0\\ \tau_{xz}\\ \tau_{yz}\\ \tau_{zz}\\ u\tau_{zx}+v\tau_{zy}+w\tau_{zz}+k_e\frac{\partial T}{\partial z}\end{pmatrix}$$

where $\mathbf{B}=(0,0,B)$ is the magnetic flux density, $\mathbf{E}=(E_x,E_y,E_z)$ the electric field, e the total energy of the gas, $\mathbf{J}=(J_x,J_y,J_z)$ the electric current density, p the static pressure, T the static temperature, t the time, $\mathbf{u}=(u,v,w)$ the gas velocity, ρ the mass density, k_e the effective thermal conductivity, and τ the viscous stress tensor with coefficients of effective viscosity.

Electrodynamics

The three-dimensional steady Maxwell equations, the continuity equation of electric current, and the generalized Ohm's law are used for the basic equations of the electrodynamics, where the induced magnetic field is neglected because the magnetic Reynolds number is much smaller than unity.

$$\nabla\times\mathbf{E}=0, \qquad \nabla\cdot\mathbf{J}=0 \tag{2}$$

$$\begin{aligned}J_x&=\frac{\sigma}{1+\beta^2}\left\{(E_x+vB)-\beta(E_y-uB)\right\}\\ J_y&=\frac{\sigma}{1+\beta^2}\left\{(E_y-uB)+\beta(E_x+vB)\right\}\\ J_z&=\sigma E_z\end{aligned} \tag{3}$$

where $\beta$is the Hall parameter and σ the electrical conductivity.

The electrical potential function ϕ is introduced with the following relations,

$$E_x=-\frac{\partial\phi}{\partial x},\quad E_y=-\frac{\partial\phi}{\partial y},\quad E_z=-\frac{\partial\phi}{\partial z}=0 \tag{4}$$

and the following partial differential equation is obtained.

$$\begin{aligned}&\frac{\partial}{\partial x}\left\{\frac{\sigma}{1+\beta^2}\left(-\frac{\partial\phi}{\partial x}+\beta\frac{\partial\phi}{\partial y}+\beta uB\right)\right\}\\ &+\frac{\partial}{\partial y}\left\{\frac{\sigma}{1+\beta^2}\left(-\beta\frac{\partial\phi}{\partial x}-\frac{\partial\phi}{\partial y}-uB+\beta vB\right)\right\}\\ &+\frac{\partial}{\partial z}\left(-\sigma\frac{\partial\phi}{\partial z}\right)=0\end{aligned} \tag{5}$$

Thermodynamical properties

Thermodynamic properties such as enthalpy and electrical conductivity are separately calculated under the assumption of thermal equilibrium, where the experimentally inferred combustion efficiency is used. Approximate functions for the temperature and the pressure for these properties are made from the calculation results. The scramjet combustion reactant mixtures were specified by the test flow rates as summarized in Ref. (3). It should be noted that the conductivity strongly depends on the gas temperature and approaches to almost zero below 2000 K.

2.2 Numerical schemes

The gasdynamical equation (1) is discretized with the finite volume method, and the Harten-Yee explicit TVD scheme[6)] is implemented for the convection terms and the second order central difference scheme is used for the diffusion terms.

The electric potential equation is discretized by using the Galerkin finite element method with the first order tetrahedron elements[7)]. The obtained linear equation is solved with Bi-CGSTAB2[8)].

3. Numerical Results

3.1 MHD channel and calculation conditions

The MHD generator channel studied is of the diagonal conducting sidewall (DCW) design using heat sink, window frame electrodes as shown in Fig.1. There are a total of thirty-three (33) active electrodes along the length of the channel inclined at 60° from the horizontal. The electrodes were fabricated from ½ inch thick copper plate, and segmentation for the channel is provided by 1/8 inch ceramic impregnated inter-electrode insulators/gaskets. The diagonal inclination gives rise to an electrode pitch (electrode and gasket projected thickness along the horizontal) of 1.8 cm. The MHD generator channel was loaded end-to-end as is typical for the diagonal configuration. The electrical output was consolidated using three power take-off leads on the front (first three electrodes) and back (last three electrodes) ends of the channel. Gross load dump current and voltage, and eight voltage differentials distributed along the generator channels length were only measured. Figure 2 depicts the MHD channel shape and the coordinate system used in the present analysis.

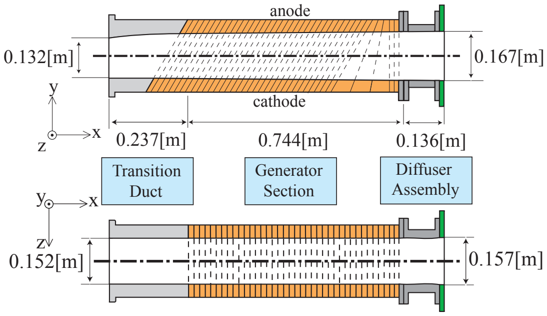

Fig. 2. Channel shape and coordinate system.

In computing the three dimensional flow field with MHD interaction, the experimental conditions obtained for Run 3 were imposed[3)]. It is given that the inlet pressure is 0.284 atm, the inlet temperature is 2480K, the inlet Mach number is 2.02, and the wall temperature is 1000 K. The maximum value of magnetic flux density is 1.48 T. Figure 3 depicts the distribution of magnetic flux density along the center line. It is assumed that the magnetic field has only the z-component, but varies in the y- and z-directions.

The analyses utilize a rather coarse grid; i.e., the electrode pitch (frame pitch) is divided with two grids, whereas the characteristic length of the arcing current (constricted current) is about 1 mm, and numerical grids of about 0.2 mm are required for all three directions in order to reveal the effects of the arcing current near walls. Modeling of arcing phenomena requires detailed three-dimensional analyses near the walls[7)], which will be carried out as a future study. The results presented herein prescribe a minimum value of the electrical conductivity in order to simulate the near-wall arcing phenomena. The approximate arcing model has two ways of limiting the electrical conductivity: (1) the minimum value is fixed to be 0.1 S/m when the electrical conductivity becomes less than 0.1 S/m ("model 1"); (2) the minimum value is the value corresponding to T of 2000K ("model 2"), when the static temperature becomes less than 2000 K. These limiting values have been decided based on the authors' experiences. It has been found that both arcing models 1 and 2 lead to almost the same results[4)], and therefore, only the model 1 is used.

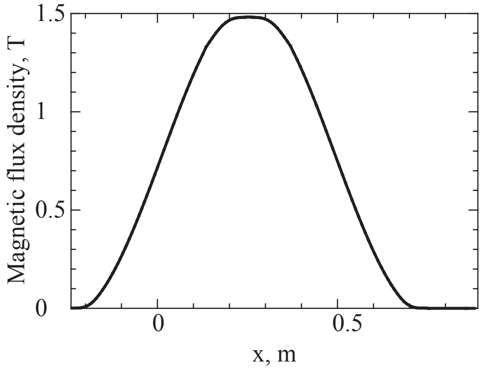

Fig. 3 Distribution of magnetic flux density.

The numerical grids consist of 128 in the x-direction, 41 in the y-direction, and 21 in the z-direction, where the symmetric feature along the magnetic field (the z-direction) is taken into account and only the half region of 0 to 0.076 m is treated in the z-direction. An even mesh is used along the x-direction with Δx of 0.9×10^{-2} m ,and the uneven meshes are used along the y- and z-direction with the minimum mesh size of Δy and Δz of 5.0×10^{-5} m on the walls. A multi-time step scheme is used in the analyses, where the largest time step is used in the core flow with Δt of 1.0×10^{-6} sec and the smallest time step is near the walls with Δt of about 1.5×10^{-8} sec, where the four domains are separately treated.

3.2 Flow field and MHD interaction parameter

The present analysis uses the experimentally measured distribution of electric potential of the electrodes (frames), as shown in Fig. 4, in order to reveal the electric current distribution that corresponds to the potential distribution. It should be noticed that the distribution of frame potential is not smooth, simply because the number of measurement ports was limited. The real potential distribution must be smooth.

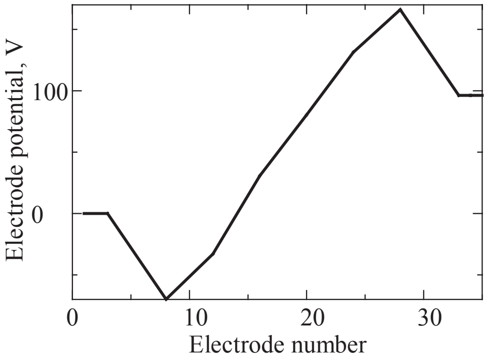

Fig.4. Distribution of electric potential (experimental data, Ref. 3).

Fig. 5 depicts the two-dimensional distribution (*x-y* plane, $z = 0$) of static pressure with MHD interaction based on Run 3 conditions, showing the expansion and compressible waves. The resultant pressure distribution with the MHD interaction is similar to the pressure distribution without MHD interaction. Little influence of MHD interaction on the flow field was anticipated because the MHD interaction is weak in this machine. The interaction parameter (based on pressure) is 0.0034 which is estimated with the following equation:

$$S_p = \frac{1}{L_x\left(P_{in} - P_{out}\right)} \int_0^{L_x} \int_0^{L_y} \int_0^{L_z} j_y B \, dxdydz \qquad (6)$$

where L_x, L_y, and L_z are the flow cross section dimensions of MHD channel along the *x*-, *y*-, and –*z*-direction, respectively.

3.3 Electrical conductivity and current conservation

The calculated load current between the 10th electrode (frame) and the 27th electrode becomes almost the same level, however, it is still seen to be substantially elevated above that of the measured current. To introduce a means of getting the three dimensional MHD generator model to more closely match the measured current, we have introduced a deficit on the ideal scalar electrical conductivity which enforces a reduced internal plasma impedance. The conductivity deficit factor, δ, is defined according to the following,

$$\delta = \frac{\sigma}{\sigma_{Ideal}} \qquad (7)$$

where σ_{Ideal} represents the thermo-chemical equilibrium level of scalar conductivity.

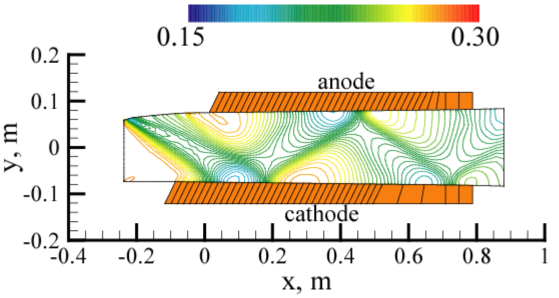

Fig. 5 Distribution of static pressure (x-y plane, z = 0.0m with MHD).

In follow-up parametric study of the effect of δ on results, it has been determined that a value of 0.813 provides a good agreement between the calculated current and the measured current. It is not clear to the authors as to why the effective electrical conductivity must be reduced from its ideal value to obtain the matching needed. However, this is not an unusual observation and in reality the ability to achieve the ideal thermo-chemical equilibrium scalar conductivity in a scramjet combustion process (where some unburned species will be present) cannot be anticipated. Along with this observation, other processes, such as non-uniform mixing, non-uniform seed dispersion, and temperature non-uniformity also can be expected to reduce the actual experienced scalar conductivity.

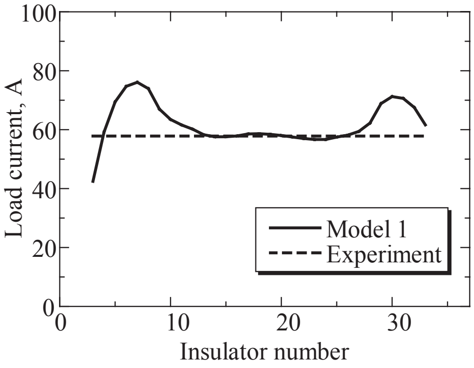

Fig. 6 Distribution of computed generator current compared to experimental measured current.

Fig. 6 shows the distribution of the calculated load current with δ of 0.813 compared to the experimental measured level. This figure illustrates a good agreement between computed current and measured current in the active part of the MHD generator channel. In the end regions of the generator channel (including the PTO electrodes) the computed current becomes higher than the measured load current with about 30% at the inlet PTO region and about 20% at the outlet PTO regions. This behavior is believed to be due to the inability to precisely specify the diagonalization angle in these regions because of the geometry where the electrode frames attach to the interface ducts.

3.4 Electrode voltage drop and current distributions

The voltage drop seen in the near electrode regions is induced as the current passes through the cold wall boundary layer. The calculations indicate sizable electrode voltage drops on the order of 50 volts of each side. It is noted that the degree of voltage drop computed is driven by both the arcing model and by the imposed 1,000 K wall temperature.

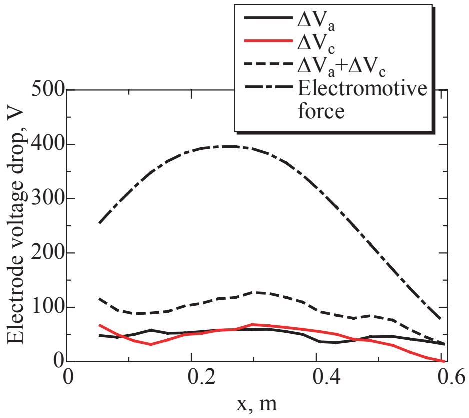

Fig. 7 Distribution of calculated electrode voltage drop.

Figure 7 shows the distribution of the voltage drop and the electromotive force along the generator channel length, where ΔVa and ΔVc are the voltage drop near the anode and cathode wall, respectively. The overall voltage drop is on the order of 100 volts. This is considered a reasonable level for this scale machine but is also sizable in comparison to the electromotive force.

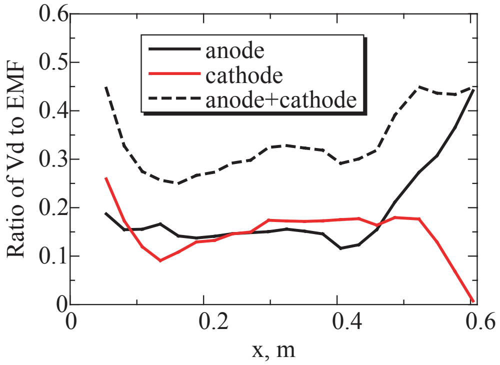

Fig. 8 Distribution of ratio of calculated electrode voltage drop.

The ratio of the electrode voltage drop relative to the electromotive force is depicted in Fig. 8, indicating a voltage loss from the induced voltage of about 30%.

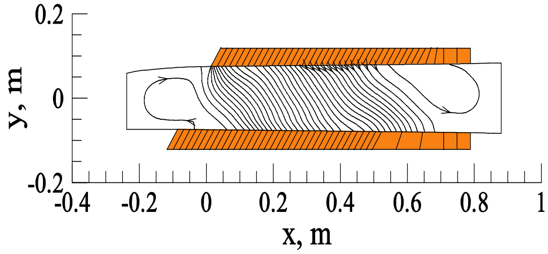

Fig. 9 Distribution of electric current on x-y plane (z =0 location).

Fig. 9 illustrates the distribution of electric current on the *x-y* plane with $z = 0$. It should be noticed that the lines in this figure illustrate a projection of the current on the *x-y* plane and are not the current stream function The distribution indicates that eddy currents are induced in both PTO end regions. Also, it is apparent that a rather large axial component of the current is induced in the active MHD region which indicates that the loading condition is not optimized.

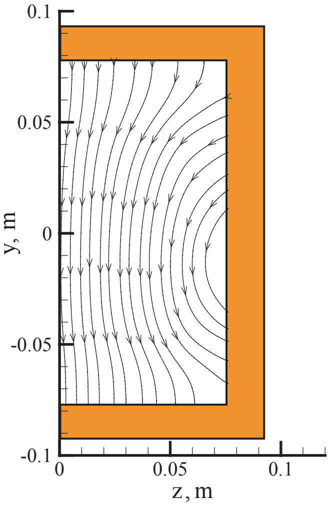

Fig, 10. Distribution of electric current on y-z half-plane at x = 0.34 m.

Fig. 10 shows the distribution of electric current on a half of the *y-z* plane at the center along the *x*-direction with $x = 0.34$ m. The current is seen to flow in and out of the sidewall. This is due to the DCW MHD generator channel design and there are several conductive electrode frames at different potential on the sidewall of channel. It also should be noticed that the current from the sidewall constricts the current from the anode, resulting in another form of non-uniformity of the current on the y-z plane.

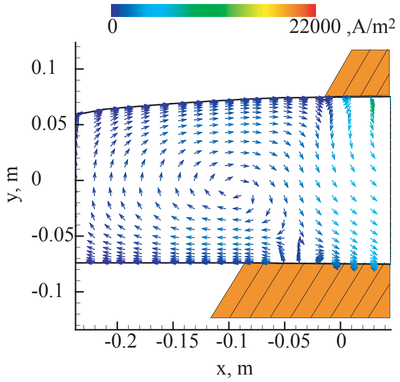

Fig.11. Distribution of electric current in the entrance PTO region on x-y plane.

Fig. 11 depicts the distribution of electric current near the entrance PTO region on the *x-y* plane. This figure shows detail of rather strong eddy-like current that is induced in the entrance PTO region. This eddy-like current may interact with the load current running in and out of the PTO frames, resulting in power degradation. However, modeling of the electrodynamics in the end regions is not enough and more detailed analysis is required to be able to define power loss effects in PTO regions.

4. Concluding remarks

The experimental scramjet driven MHD generator developed under the Hypersonic Vehicle Electric Power System (HVEPS) program has been numerically analyzed by the authors using our three dimensional MHD generator computer code. The experimental conditions and results analyzed were those described for the HVEPS MHD power demonstration test Run 3 as taken from Reference 3. The analysis was addressed using a fully coupled three dimensional computer code consisting of the time-dependent Navier-Stokes equations, the steady Maxwell equations subject to the MHD approximation, and the thermo-chemical equilibrium equations.

The following conclusions and comments are obtained:

(1) The MHD interaction is small for this small scale test facilities and the operating conditions, resulting in the MHD interaction parameter based on pressure of 0.0034. Perturbation of the flow field due to MHD interaction is, therefore, negligible.

(2) A very good agreement has been obtained between the experimental and numerical results for the generator performance in the active MHD region when an scalar electrical conductivity deficit of 0.813 was applied to the thermo-chemical ideal value. The reason of the effective reduction of electrical conductivity on the order of about 19 % is not clear but is considered plausible due to some level of incomplete combustion and flow field non-uniformities.

(3) A relatively large electrode voltage drop near the anode and the cathode of about 100 volts overall has been obtained with the ratio with the induced electromotive force in the range of about 0.3 in the active region. The absolute value of this ratio is considered reasonable by the authors for this size machine and will be substantially alleviated in a large MHD generator.

(4) The present three dimensional MHD generator computer code has fairly well reproduced the very large electrical losses that were seen in both entrance and exit PTO regions, as evidenced in the experimental data. More detailed calculations with refinement of the electrodynamics, however, seem required and these are planned as a future study. However, the end region power losses are primarily a manifestation of the rapid decay in the magnetic field in these regions which drive a reversal of the Hall electric field. This is avoidable with proper design of the PTO circuitry.

Acknowledgments

The authors wish to acknowledge Dr. John Lineberry, LyTec for his valuable discussion, and Professor T. Iwashita, Kyoto University and Mr. T. Yoshino, University of Tsukuba who helped us to develop the computer code related to Bi-CGSTAB2.

References

[1] J. T. Lineberry, L. Begg, J. H. Castro, R. J. Litchford, 37th AIAA Plasmadynamics and Lasers Conference, AIAA-2006-3080 (2006).

[2] J. T. Lineberry, L. Begg, J. H. Castro, R. J. Litchford, 14th AIAA/AHI International Space Planes and Hypersonic Systems and Technologies Conference, AIAA-2006-8010 (2006).

[3] J. T. Lineberry, L. Begg L,J. H. Castro, R. J. Litchford, J. M. Donohue, 38th AIAA Plasmadynamics and Lasers Conference, AIAA-2007-3881 (2007).

[4] D. Gotoh, T. Takahashi, T. Fujino, M. Ishikawa, J. T. Lineberry, 16th International Conference on MHD Energy Conversion, AIAA-2007-4015 (2007).

[5] H. W. Stock, W. Haase: 19th AIAA Fluid Dynamics, Plasmadynamics and Lasers Conference, AIAA-87-1302 (1987).

[6] H. C. Yee, A. Harten: AIAA Journal **25**, (2), 266 (1986).

[7] M. Ishikawa, K. Itoh, K. Tateishi, 33rd AIAA Plasmadynamics and Lasers Conference, AIAA-2002-2237 (2002).

[8] M. H. Gutknecht, SIAM journal on scientific computing **14** (5), 1020 (1993).

---

*Corresponding author: misikawa@kz.tsukuba.ac.jp